iScience

CellPress
OPEN ACCESS

Article

Enhanced Optical Fiber for Distributed Acoustic Sensing beyond the Limits of Rayleigh Backscattering

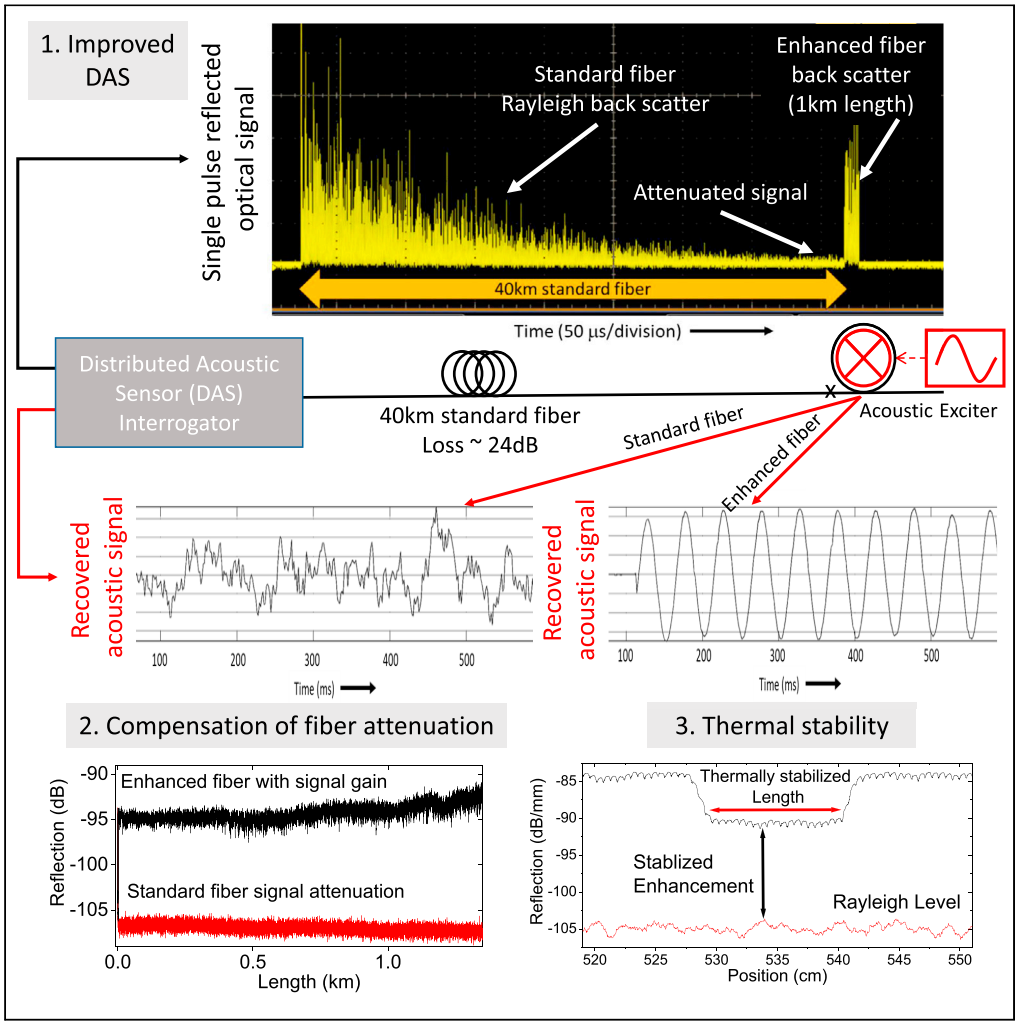

Paul S. Westbrook, Kenneth S. Feder, Tristan Kremp, ..., Mohammad Karimi, Anthony Nkansah, Alan Yau

westbrook@ofsoptics.com

HIGHLIGHTS

Enhanced fiber with compensation of sensor signal attenuation over more than 1 km

Measurement of UV-induced change in fiber Kerr nonlinearity over 1 km

Thermal stability of UV-induced enhancement for 3 weeks at 210°C

Enhanced fiber leads to higher spatial resolution in distributed acoustic sensing

Westbrook et al., iScience 23, 101137
June 26, 2020
https://doi.org/10.1016/j.isci.2020.101137

iScience

CellPress
OPEN ACCESS

Article

Enhanced Optical Fiber for Distributed Acoustic Sensing beyond the Limits of Rayleigh Backscattering

Paul S. Westbrook,[1,5,*] Kenneth S. Feder,[1] Tristan Kremp,[1] Eric M. Monberg,[1] Hongchao Wu,[1] Benyuan Zhu,[1] Lei Huang,[4] Debra A. Simoff,[2] Scott Shenk,[1] Vincent A. Handerek,[3] Mohammad Karimi,[3] Anthony Nkansah,[3] and Alan Yau[3]

SUMMARY

We report on engineered fibers with enhanced optical backscattering that exceeds Rayleigh scattering limits by more than one order of magnitude. We measure attenuation less than 0.5 dB/km from 1,300 to 1,650 nm. By controlling the enhanced backscatter over a 1.5-km length, we compensate for this attenuation, resulting in a higher backscatter signal at the end of the fiber. We demonstrate that the scattering strength may be stabilized for operation at temperatures above 200°C for at least 3 weeks. We show that the deleterious signal distortion due to the Kerr nonlinearity is within 10% of standard fiber. We then report on the use of these fibers in distributed acoustic sensing (DAS) measurements. A significant increase in acoustic signal-to-noise ratio leads to the possibility of improved spatial resolution in the enhanced fiber DAS system.

INTRODUCTION

Optical fibers are uniquely suited to distributed sensing applications (Bao and Chen, 2012; Hartog, 2017). Lengths in excess of 1 km are readily fabricated into cables and can provide information about temperature, strain, and acoustics without the requirement for electrical connections, and with the possibility of resistance to harsh environmental conditions in various structures. Examples of sensing systems include distributed temperature (Gifford et al., 2005; Sancho et al., 2013), strain (Froggatt and Moore, 1998) and acoustic sensing (Daley et al., 2013; Kirkendall et al., 2007; Diamandi et al., 2019), as well as sensing of bend and shape (Gander et al., 2000; Duncan et al., 2007; Ahmad et al., 2019). A critical aspect of such systems is that they rely on backscattering of light propagating in the core of an optical fiber, usually in single-mode operation. Backscattering can be used with many types of sensor interrogators, including optical frequency domain reflectometry (OFDR) (Eickhoff and Ulrich, 1981; Soller et al., 2005) and coherent optical time domain reflectometry (OTDR) used in distributed acoustic sensing (DAS), which is also known as distributed vibration sensing (DVS) (Shatalin et al., 1998; Posey et al., 2000; Koyamada et al., 2009; Parker et al., 2014). A DAS sensor system converts the entire length of an optical fiber into a distributed microphone. Acoustic sensing is accomplished by launching highly coherent pulses into the optical fiber and collecting the backscattered light with very sensitive detectors. When acoustic waves compress or elongate the optical fiber, the backscattering signal shows slight changes due to the change in optical path length. By comparing the backscatter from successive pulses, it is possible to reconstruct the acoustic wave propagating along the fiber. DAS interrogator development has made such distributed sensors competitive with other sensors such as three axis fiber point sensors (Bostick, 2000) and conventional electromechanical geophones (Daley et al., 2016). Their primary advantages over point sensors is lower cost of deployment, compact form factor, and the very long continuous distributed sensing profile they can offer, which allows, for instance, the observation of seismic wave propagation along the sensor fiber with resolution of a few meters. This capability has been demonstrated in various applications including seismic monitoring of oil and gas facilities (Daley et al., 2013; Mateeva et al., 2014; Hartog et al., 2014), security systems (Owen et al., 2012), telecom networks (Wellbrock et al., 2019), earthquake detection (Lindsey et al., 2017), as well as rail (Cedilnik et al., 2018) and pipeline (Tanimola and Hill, 2009) monitoring. Such systems can be implemented over lengths in excess of 40 km of standard fiber, and the output can be interpreted with various algorithms giving information about mechanical faults, fluid flow, seismic activity, vehicle traffic, security intrusions, and other disturbances. Increasingly, sophisticated algorithms using deep learning and other data science techniques are being applied to the large data output from these applications (Westbrook, 2020). The crucial backscattering signal is usually caused by the

[1]OFS Labs, Somerset, NJ, USA

[2]OFS, Fitel, LLC, Avon, CT, USA

[3]Fotech Solutions Ltd., Fleet, Hampshire GU52 0RD, UK

[4]Legrand, North America, Avon, CT, USA

[5]Lead Contact

*Correspondence: westbrook@ofsoptics.com

https://doi.org/10.1016/j.isci.2020.101137

inherent Rayleigh scattering that is a universal signal present in all optical fiber waveguides and at all wavelengths. Rayleigh scatter requires no additional processing of the fiber, and it is spatially continuous, thereby giving complete coverage over any waveguide length. However, the primary drawback is that the Rayleigh backscattering signal is very weak. For DAS/DVS, the weak signal limits acquisition speed and reach. It would be very useful to improve the signal-to-noise ratio while still maintaining the advantages of having a continuous backscattering sensor signal, low attenuation, and low cost per length of fiber. Rayleigh backscattered power can be increased by raising the numerical aperture (NA) of the fiber, since this improves the capture fraction for backscattered light. Adding extra dopants can also increase scattering, but this approach typically worsens the attenuation of the fiber, negating some of the benefits. Moreover, there are limits to the increase in NA that is possible due to the requirement for single-mode propagation and practical limits on dopant concentrations. Typically, such an approach can yield only 3- to 6-dB gain in Rayleigh scattered power while increasing attenuation substantially. Other approaches to strengthening the backscatter involve various remote amplification schemes (Wang et al., 2014); however, these add cost and complexity to a system. Such approaches also face nonlinear limits when the amplifier is at the input and can add additional noise when used to amplify a weak signal at the output of the fiber. In both cases, there are limits to the increase in signal-to-noise ratio that may be obtained. In still other approaches, signals may be detected from more than one fiber core and combined into a single signal, but this increases both the cost of the sensing fiber and the complexity of the interrogation scheme. Therefore, research on other methods continues. An alternative approach involves processing the bare fiber to increase the optical backscattering. It is well known that exposure of optical fiber to pulsed radiation may increase elastic scattering well above the native Rayleigh scattering, particularly through the formation of periodic or quasi-periodic fiber Bragg gratings. While typical Bragg gratings are less than 10 cm in length, such processing may be applied over long fiber lengths and has been demonstrated in several fabrication systems using single core fibers, including direct write or point-by-point writing with UV (Asseh et al., 1997; Monet et al., 2019) and IR femtosecond lasers (Lu et al., 2019), reel-to-reel setups (Lefebvre et al., 2006), drum systems (Brennan et al., 2003), draw tower grating fabrication (Askins et al., 1994; Bai et al., 2015; Zaitsev et al., 2016; Guo et al., 2013), as well as direct UV exposure (Westbrook, 2016; Loranger et al., 2015). We have reported on an alternative and flexible method to achieve nearly continuous backscattering over many meters in fibers with any number of cores using reel-to-reel fiber handling and a UV transparent coating (Atkins et al., 2002; Westbrook et al, 2014, 2015, 2017a, 2017b). Recently this approach was extended to fibers with lengths in excess of 1 km (Westbrook et al., 2017b). This work demonstrated a more than 10-dB increase in optical backscattering over the native Rayleigh scattering of the optical fiber. Typically, such UV processing is expected to increase the fiber attenuation, thereby reducing the backscattering enhancement. However, this work showed less than 0.1-dB/km increase in attenuation after the UV irradiation. In subsequent work it was shown that the increased optical signal-to-noise ratio also gave increased acoustic signal-to-noise ratio in DAS measurements (Handerek et al., 2018). We note, however, that these enhanced scattering fibers still showed attenuation, thus exhibiting signal degradation. Since these fibers are processed with UV radiation along their length, it should be possible to completely eliminate the degradation of signal due to fiber attenuation by controlling the UV exposure. Moreover, although the linear attenuation was promising for applications, as described above, it is also important to verify that the nonlinear properties of the fiber are not degraded by the exposure to UV radiation. In lengths of fiber typical of DAS and other applications, which can be in excess of 10 km, it is important to use the highest possible input power to ensure good signal-to-noise performance in any given sensing scheme. It is therefore important to ensure that any scattering enhancement can be achieved without increasing various nonlinear effects in the fiber. Moreover, the thermal stability of the very small UV-induced index perturbations giving rise to our scattering enhancements must also be verified, as it is well known that UV-induced changes in optical fibers can degrade over time at high temperatures (Erdogan et al., 1994). Studies of single shot gratings written into highly photosensitive fibers have been published (Bartelt et al., 2007); however, the thermal stability of ultra-weak gratings written into the low loss, low Ge doped standard single mode fibers that we consider in our work has not been discussed in detail.

In this work, we report measurements of enhanced scatter fibers that address these concerns and thereby demonstrate that these fibers are robust candidates that can enable improved sensing. We characterize the Kerr effect in a 1-km length of UV-processed fiber. We compare our results with a length of fiber from the same fiber draw but without any UV exposure and find that the low nonlinearities of a G.652 standard single mode fiber are maintained. We also show that the level of scattering may be controlled by varying the UV dosage on the fiber and that the dosage may be varied along the fiber length to cancel the attenuation of the optical fiber. We report on the attenuation of our arrays from 1,300 to 1,600 nm. We show that the attenuation in this wavelength range can be less than 0.5 dB/km. We also present data on the thermal

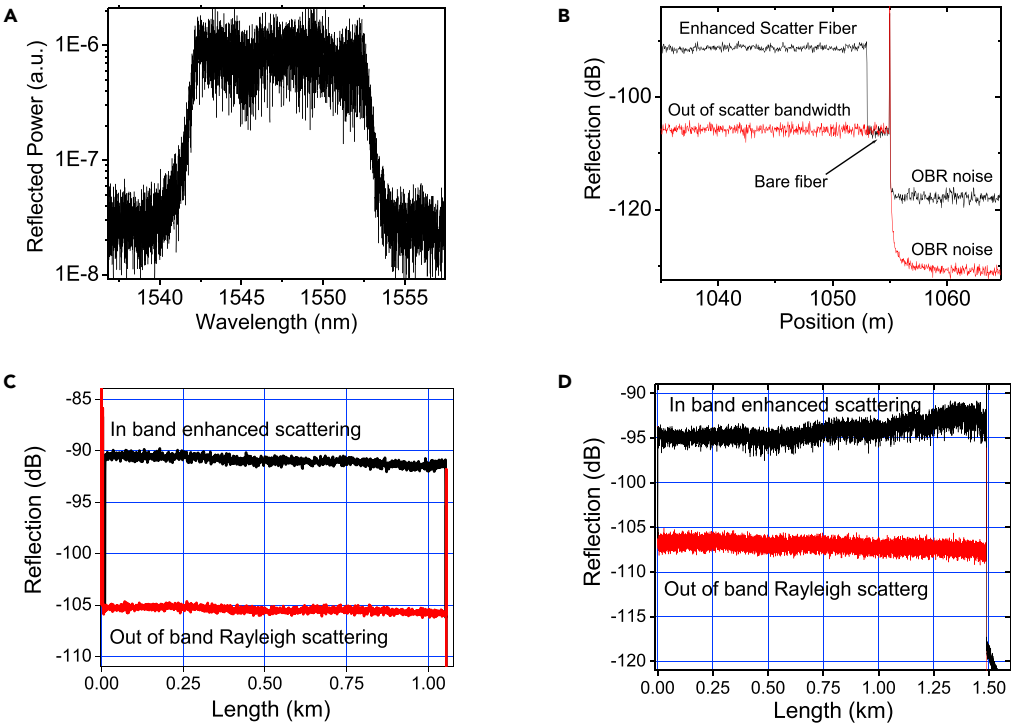

Figure 1. Enhanced Scatter Fiber Measurements

(A) Spectrum of the backscattered light measured over 10 cm of enhanced fiber.

(B) Backscattered power measured at 1,550 (black) and 1,526 nm (red), outside of the scattering bandwidth. Bare fiber section indicates the Rayleigh scattering level of the fiber; ~14 dB enhancement in backscattering is observed. OBR noise level measured after fiber end is indicated.

(C) Extended range measurement using the LUNA OBR. The black curve is measured at 1,550 nm where there is enhancement in scattering. The red curve is measured at 1,526 nm and is close to the bare Rayleigh scattering level. Both curves show the attenuation that results in lower signal at the end of the fiber.

(D) A 1.4-km array showing increasing backscattered power over the entire length of the array, which overcompensates the attenuation of the fiber, giving more signal at the end of the fiber. For comparison, an OBR trace at 1,600 nm outside of the scattering bandwidth is shown. Like the traces in Figure 1C, this trace decreases in strength along the fiber owing to fiber attenuation.

stability of the enhanced fiber at temperatures above 150°C. Finally, we show that the DAS backscatter signal may be improved over kilometer lengths, entirely overcoming the attenuation from 40 km of standard fiber. We present the improvements in acoustic signal-to-noise ratio obtained from the increased optical signal-to-noise ratio and show that these improvements can be exploited to improve spatial resolution in DAS.

Enhanced Scattering Fiber Properties

Our fiber was prepared through UV processing as described in Westbrook et al., 2017a). Quasi-continuous, incoherent scattering over a bandwidth of 10–20 nm was created with exposure of the fiber to a 248-nm pulsed excimer interferogram. Importantly, such exposure requires only a few pulses resulting in an exposure level of 10–30 mJ/cm^2. Moreover, the 10- to 20-ns pulse width and diffractive phase mask optics used to generate the index modulation in the core of the fiber are very robust to changes in the optical alignment and even allow for the fiber to be moving during the exposure. As a result, our enhanced fiber can be fabricated using a reel-to-reel process or in-line during the fiber draw process when the fiber is moving at speeds approaching 1 m/s. Such rapid processing is critical to the commercial viability of enhanced fibers for distributed sensing, since it is important that very large lengths of the fiber can be fabricated for DAS applications that often require up to 40 km of fiber in a single application. When used in a reel-to-reel system, our process is highly scalable, allowing for gratings of any length and a precise variation of the exposure conditions to control the backscattered light. We report on two such enhanced fibers in Figures 1C and 1D. In general, UV processing conditions depend on the fiber and UV source used and are adjusted to meet

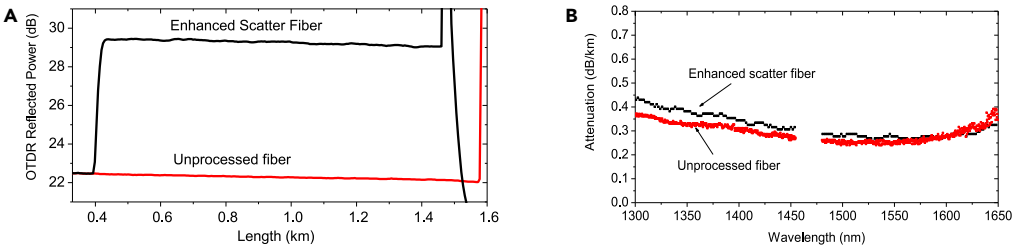

Figure 2. Enhanced Scatter Fiber Attenuation

(A) Attenuation of the enhanced optical fiber. OTDR traces of the processed and unprocessed fibers.

(B) Fiber attenuation over 1.2 km for the enhanced fiber and the unprocessed fiber. A spectral artifact near 1,460 nm was removed for clarity.

a particular specification by inscribing a series of test exposures. For Figure 1C, the UV fluence was 27 mJ/cm^2, interferogram length was 14 mm with approximate chirp rate of 7 nm/cm, and a displacement between exposures of 5 mm. The fiber shown in Figure 1D had exposure conditions of 20 mJ/cm^2 every 7 mm using an interferogram of 35 mm in length and a chirp rate of 6.5 nm/cm. As discussed below, the exposure level increased by approximately 20% over the length of this fiber, making the enhancement increase to compensate for the fiber attenuation.

After inscription, the fiber may be characterized using several optical measurements. It is first measured using optical frequency domain reflectometry (OFDR, also known as swept wavelength interferometry, SWI) with a LUNA OBR. Because the OFDR technique records a high-resolution spectrum, we can obtain the spectral shape of the fiber enhancement by measuring a short length. Figure 1A shows the reflection spectrum of 10 cm of the enhanced fiber from an OFDR measurement with a scan range of 20 nm centered at 1,547 nm. A 10-nm enhanced scattering bandwidth is observed. We then used the extended range setting on the OBR to measure the full 1-km array. Since this requires a reduced OBR scan range of only 0.8 nm, it could not give a full optical spectrum. Measurements were performed within the bandwidth at 1,550 nm and outside the scattering bandwidth near 1,526 or 1,600 nm. This out-of-band measurement is very close to the Rayleigh scatter level of the unprocessed fiber as is apparent in Figure 1B, which includes a short length of unprocessed fiber exhibiting only Rayleigh scattering. A comparison between the in-band and out-of-band signals in Figure 1B gives a measure of the backscatter enhancement, which is approximately 14 dB for this fiber. Figure 1C then shows the full scan of the backscattered power versus position over the 1-km fiber length at both 1,550 and 1,526 nm. The enhanced scatter is observed over the entire length of the fiber. We also note that the decrease in (round trip) backscattering signal from the beginning to the end of the 1-km fiber length was less than 1 dB, almost unchanged from the bare fiber before grating inscription.

Although this enhanced fiber still showed a decrease of signal along its length, this attenuation can be overcome by ramping the strength of the exposure along the fiber. Another length of enhanced fiber was therefore fabricated for which the strength of exposure and hence the scattered power along the length of the optical fiber was increased along the length of the fiber. The back reflection depends on the level of UV used to process the optical fiber. A 1.4-km length of fiber was processed to give a 1-dB overall increase over the entire length of the fiber. Therefore, this length of fiber showed an effective increase of the optical scattering along the fiber. The OBR trace for this fiber is shown in Figure 1D. Also shown in Figure 1D is a scan performed at 1,600 nm, which was outside of the scattering bandwidth. This trace shows the fiber attenuation, which is similar to that of both the in-band and out-of-band scattering observed in Figure 1C. Thus, the backscattering signal in this fiber has exceeded the limits set by fiber attenuation.

The scattering fibers may also be characterized with OTDR. Figure 2A shows OTDR traces of the scattering fiber. The observed enhancement in scattering level is approximately half that in Figure 1C because of the factor of two applied to convert round trip to single-pass attenuation. We also note that, if the OTDR bandwidth does not overlap fully with the enhancement bandwidth, the backscatter observed would be a mixture of Rayleigh and enhanced backscatter, giving rise to some error in measuring the discrete increase in signal at the start of the scatter fiber. For the distributed attenuation, the OTDR trace for the enhanced fiber has a slope only slightly lower than that for the untreated fiber. Comparing these traces, we can estimate that UV processing increased the fiber attenuation from about 0.3 to about 0.4 dB/km. In order

Fiber		Attenuation at 1,550 nm (dB/km)	Aeff @ 1,550 nm (μm^2)	Fiber Length (km)	Average n_2 (m^2/W)
Enhanced Scatter	Out of band	0.40	82	1.04	2.370E-20
Enhanced Scatter	In band	0.40	82	1.04	2.468E-20
Unprocessed		0.28	82	1.0	2.283E-20

Table 1. Nonlinear Kerr Coefficient n_2 of the Enhanced Scattering Fiber Compared with Unprocessed Fiber

to obtain a more accurate measurement of the fiber attenuation, a spectral loss measurement was performed using a standard cutback method. The result of this measurement is shown in Figure 2B. We observe that the loss from 1,300 to 1,650 nm is less than 0.5 dB/km in the processed fiber.

Long lengths of optical fiber can exhibit very low thresholds for various nonlinear effects. Such effects are well known and place limits on applications in telecom and sensing that use long lengths of optical fiber. In particular, DAS can be performed over lengths up to 40 km. Therefore, any modification of the optical fiber must be performed while maintaining acceptable limits on the nonlinear behavior. To test the enhanced scattering fiber, we measured the value of the Kerr coefficient n_2 for the enhanced scattering fiber both inside and outside the enhanced scattering bandwidth, and we also compared this to a length of unprocessed fiber. The nonlinear Kerr coefficient n_2 was obtained using a measurement of the nonlinear phase shift induced through the self-phase modulation (SPM) effect. Briefly, a continuous wave dual-wavelength beat signal was used as a pump signal and the value of n_2 was extracted from a measurement of the ratio between the fundamental beat note and first side band developed as a result of the SPM (Boskovic et al., 1996). The fiber parameters and n_2 values are shown in Table 1. For signals within and outside of the enhanced scattering window, the n_2 value was larger than in the unprocessed fiber by a few percent. Such an increase is not expected to have significant impact on the performance of the fiber in sensing applications.

Optical Backscattering Figure of Merit

Although our UV-processed fibers show increased backscattering, it is also well known that UV exposure can increase the attenuation of the fiber (Askins and Putnam, 1997). In fact, any change to the waveguide that increases backscattering, such as a change in core composition, can also increase fiber loss. If the attenuation increases more than the increase in backscattering then there will be no improvement in the signal-to-noise ratio when using such a fiber. As a result, it is important to quantify the degree to which a given enhanced scattering fiber has actually increased the total backscattered signal used in the sensing applications.

To arrive at a useful figure of merit valid across all enhanced scattering fibers we seek to separate the waveguiding properties and the inherent scattering. To accomplish this, we consider an ideal fiber, which exhibits only Rayleigh scattering. In such a fiber, the backscattered signal and the fiber attenuation may be related as follows:

$$R_{\text{backscatter}}^{(\text{Rayleigh})} = \alpha_{\text{Rayleigh}} S. \qquad \text{(Equation 1)}$$

Here α_{Rayleigh} is the Rayleigh scattering coefficient (in unit 1/m), which depends on perturbations of the fiber refractive index frozen into the glass matrix during the fiber fabrication. These perturbations occur over a very large range of length scales and give rise to scattering in all directions, both out of the guiding core and back into it. The dimensionless factor S is the capture fraction and depends on the fiber waveguide. S is related to the fraction of scattered light that remains guided in the fiber core. It depends primarily on the numerical aperture NA of the fiber, since this governs the maximum incidence angle of light that experiences total internal reflection at the boundary of the core and cladding. Therefore, to compare backscattering enhancement across different fiber waveguides, we would like to remove the dependence on S while comparing actual attenuation and backscattering measured for a given fiber. However, S is a complicated function of the waveguide parameters. We therefore require an approximate expression for S that depends only on measurable waveguide parameters such as the NA, modal effective index, and core diameter.

We may express the capture fraction S as follows: $S = \eta\left(\frac{NA}{2n}\right)^2$, where NA is the numerical aperture of the fiber, n is the refractive index of the core, and the dimensionless factor η depends on waveguide properties

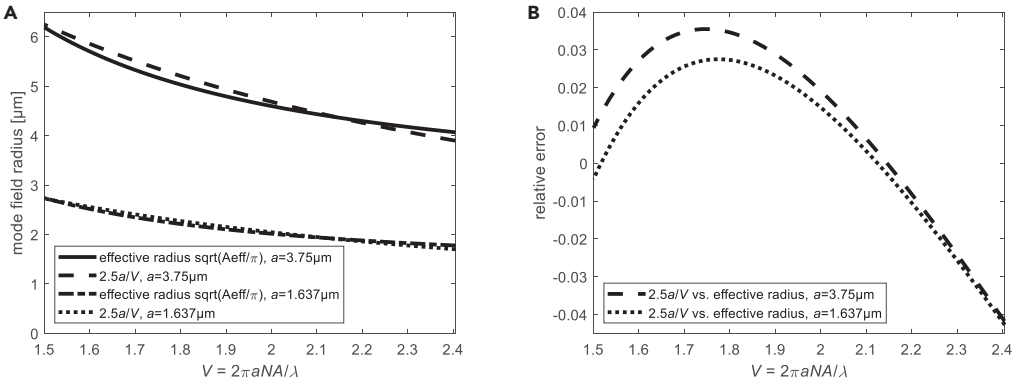

Figure 3. Relationship between Mode-Field Radius and Waveguide Parameters

Mode-field radius of step-index fibers in the relevant single-mode interval $1.5 \leq V \leq 2.405$ with core radii 3.75 and 1.637 μm, respectively, and numerical apertures 0.132 and 0.301, respectively.

(A) $r_0 = \sqrt{A_{\text{eff}}/\pi}$ and approximation $2.5a/V$.

(B) Relative error $2.5a/(r_0 V)$-1.

such as the core radius a and on modal properties at the operating wavelength λ. For graded-index and step-index multimode fibers, we have $\eta = 1$ and $\eta = 1.52$, respectively (Nakazawa, 1983) (Personick, 1977). For a step-index single-mode fiber with core radius a and normalized frequency $V = 2\pi aNA/\lambda$, the mode-field radius r_0 (with effective area $A_{\text{eff}} = \pi r_0^2$) at the wavelength λ in the relevant single-mode regime $1.5 \leq V = \frac{2\pi a}{\lambda} NA \leq 2.405$ can be approximated by $r_0 \approx 2.5a/V$ with a relative error of less than 4%, see Figure 3.

Thus, in a step-index single-mode fiber, the capture fraction can be approximated according to (Nakazawa, 1983)

$$S = \frac{3}{2}\left(\frac{a\,NA}{r_0 V n}\right)^2 \approx \frac{3}{2}\left(\frac{NA}{2.5 \cdot n}\right)^2 = 0.96\left(\frac{NA}{2n}\right)^2, \qquad \text{(Equation 2)}$$

corresponding to $\eta \approx 0.96$. The capture fraction obviously varies only weakly as a function of waveguide design. According to Equation 1, increased backscattering can be achieved either by increasing α_{Rayleigh} through the addition of more index perturbations or by increasing the capture fraction, primarily through increasing the NA in Equation 2.

With this understanding of the relationship between S and the waveguide parameters, we define a *backscattering figure of merit*:

$$FOM = \frac{R_{\text{backscatter}}}{\alpha_{\text{fiber}}\left(\frac{NA}{2n_{\text{eff}}}\right)^2}, \qquad \text{(Equation 3)}$$

where $R_{\text{backscatter}}$ is the relative amount of power backscattered, due to any physical effect, per unit length, and α_{fiber} is the total attenuation coefficient of the fiber arising from Rayleigh scattering, UV photodarkening, dopant concentration, or any other effects. The only waveguide parameters are the NA and effective index n_{eff} of the mode. According to the above derivation, this FOM would be unity for an ideal graded-index multimode fiber whose backscattering and attenuation are exclusively due to Rayleigh scattering. However, our analysis shows that it would be close to unity for most single-mode fibers as well.

We may estimate the FOM for the processed and unprocessed fibers in Figures 1 and 2. From the OBR measurements, for the unprocessed fiber, we obtain a value of $R_{\text{backscatter}} \approx$ -103 dB/mm = $5 \cdot 10^{-8}$/m. The spectral and OTDR fiber attenuation near 1550 nm was $\alpha_{\text{fiber}} = 0.3$ dB/km = $0.3 \cdot \frac{\log(10)}{10}$/km = $6.91 \cdot 10^{-5}$/m, and we estimate that $NA = 0.13$, and $n_{\text{eff}} = 1.45$. Thus, we obtain FOM $\approx \frac{5 \cdot 10^{-8}}{6.91 \cdot 10^{-5} \cdot \left(\frac{0.13}{2 \cdot 1.45}\right)^2} = 0.36$ for the bare fiber. The figure of merit of pristine fiber is expected to be less than unity since Rayleigh

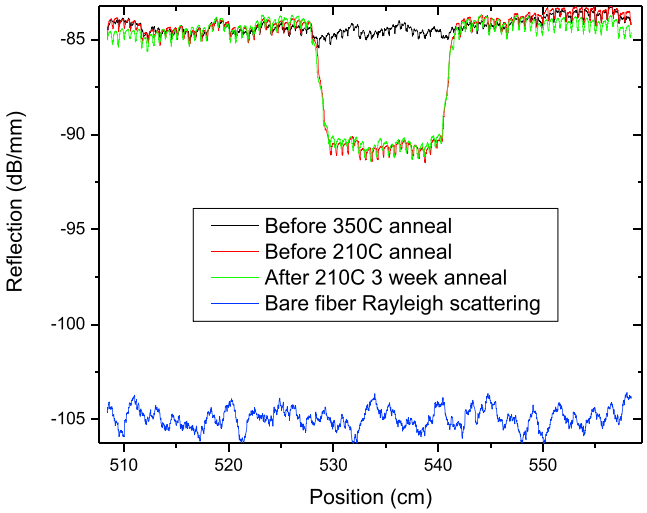

Figure 4. Thermal Stability of 13 dB Enhanced Scattering in UV-Processed Fiber

Only the region between 530 and 540 cm was treated with high temperatures. Black: Before anneal at 350°C. Red: After 350°C anneal. Green: After exposure to 210°C for 3 weeks ($2 \cdot 10^6$ s) showing no additional decay. Blue: Rayleigh scattering reference observed in the same length of fiber at 1,600 nm, outside of the enhancement bandwidth.

backscattering is not the only factor that contributes to the fiber loss α_{fiber} in Equation 3. After inscribing the grating array, we found an increase in $R_{backscatter}$ by 14 dB and an increase in α_{fiber} to approximately 0.4 dB/km. Thus, the figure of merit is $\approx 10^{\frac{14}{10}} \cdot \frac{0.3}{0.4} \cdot 0.36 = 6.8$ after the UV processing. This enhancement goes beyond any increase in backscattering that can be expected from an increase in capture fraction through waveguide design. Moreover, as shown in Figure 1D, by increasing the strength of the scattering along the fiber, we can increase the FOM along the fiber, making the optical backscatter larger at the end of the fiber to compensate for the propagation loss.

Thermal Stability of the Enhanced Fiber

Many DAS applications require thermal stability at temperatures in excess of typical telecom conditions (80°C). In some applications, the sensor must survive at temperatures as high as 150°C or 200°C. A key advantage of Rayleigh scattering is that it will exhibit minimal change at such temperatures. On the other hand, it is well known that UV-processed fiber used in sensor applications with fiber Bragg gratings shows decay with exposure to high temperatures (Erdogan et al., 1994). Most of these studies involved heavily exposed short lengths of fiber, whereas comparatively few studies have been done on weakly exposed fibers (Bartelt et al., 2007). To ensure reliability, such sensors are typically exposed to a temperature well above the operating temperature for a short period of time to guarantee stable performance at the lower operating temperatures. We therefore performed a set of annealing steps to test the thermal stability of our scattering fiber. In particular, for certain applications, stability of a fiber sensing cable at temperatures in excess of 200°C for days to weeks is required to complete testing in applications such as seismic profiling. Such cables can show degradation in various components. However, it is generally expected that performance of DAS signals will not be limited by a decay of the backscattering signals. We therefore designed an experiment to test whether our enhanced scatter fiber can survive thermal environments in this regime. We fabricated a length of the scattering fiber and performed three thermal anneals. We first annealed the fiber at 120°C for 24 h. This was then followed by a 350°C anneal for 180 s. These two stabilization anneals were then followed by a test anneal at 210°C for a period of 3 weeks, or approximately $2 \cdot 10^6$ s. For the 350°C anneal, a length of the fiber was stripped of coating and placed in a slot oven operating at 350°C. After 180 s, the oven temperature was lowered to 210°C and the grating was left inside for 3 weeks. OFDR measurements were performed using a LUNA OBR at the beginning and end of the annealing time. Figure 4 shows the OFDR scan of reflectivity versus position. The slot heater was 10 cm long, and the region annealed at 350°C appears as a decreased reflectivity level over the 10-cm range. Four OFDR scans are shown: the reflectivity before the 350°C anneal; the reflectivity after the 350°C but before the 210°C anneal; and the scan after 3 weeks at 210°C. Also shown is the Rayleigh scattering observed near 1,600 nm at the same location in the fiber. As previously discussed, this level gives a good approximation of the native

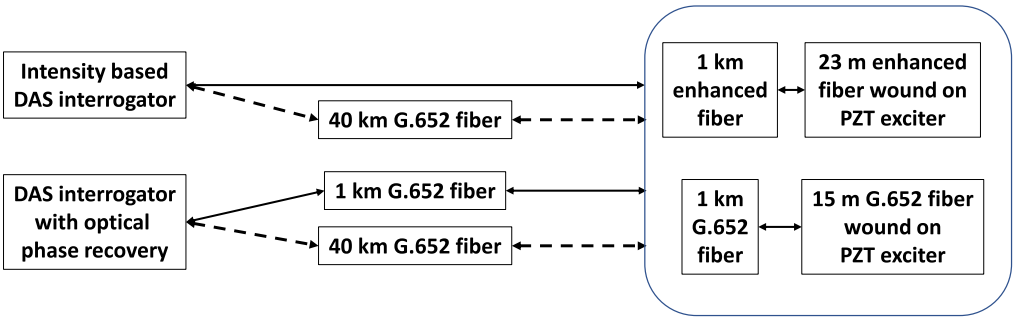

Figure 5. DAS Testing Setup

Testing used one of the two interrogators at the left. The lines indicate the optical pathways for measurements over both short (solid) and long (dashed) ranges.

Rayleigh scattering in the fiber. The difference between the Rayleigh curve and the grating curves shows that the enhancement remained at approximately 13 dB above Rayleigh scattering for the entire 3 weeks at 210°C. This shows that the enhanced scatter will be stable for timescales of at least several weeks at 210°C. It is well known that stability at lower temperature is typically exponentially longer; thus, the stability at 130°C is expected to be of the order of years.

Application in DAS

The preceding sections have discussed optical properties of the enhanced scattering fiber, whereas it is important to test this fiber in actual sensing applications. The increased optical signal is expected to increase the acoustic signal-to-noise ratio as well. Therefore, a series of tests was performed to characterize this improvement. It is important to consider two different types of DAS systems in characterizing the improvement given by the enhanced optical fiber. For most commercial DAS systems these measurements are based either on an analysis of the temporal variation of the backscattered intensity or the optical phase change at a fiber location. Phase analysis provides better linearity of response and uniformity of sensitivity along the fiber. The enhanced scattering fiber was tested in both types of detection system. Both systems used direct optical detection, with single and double pulse interrogation in the intensity- and phase-based systems, respectively. These systems were similar to those discussed in Kanellopoulos and Shatalin (2012); Handerek (2016). The test setups used are summarized in Figure 5. In all of the measurements, an ~23-m coil of enhanced scattering fiber was wound onto a piezoelectric exciter tube that was used to generate easily measurable dynamic strain signals along the fiber. These measurements were compared with signals originating from a 15-m coil of SMF-28 fiber wound onto a similar exciter. The difference in coil lengths between the two fiber types did not affect the comparison results, since the spatial resolution of the interrogation system was shorter than the coil length for all tests.

Short-range tests were performed at 1 km for the intensity-based system and 2 km for the phase-based system. For long-range testing, a 40-km length of SMF-28 fiber was placed between the interrogator and the PZT coil assembly. All tests employed a pulse repetition rate close to the maximum limited by the need to ensure that only one interrogation pulse was present in the fiber at any time. In all cases, the interrogation systems were set to 100 ns pulse width, providing 10 m spatial resolution. All tests were performed at an operating wavelength of 1,540.56 nm. The backscatter from the enhanced scattering fiber and the response to disturbance were seen to behave in a very similar manner to untreated fiber, even though the dominant component of the backscatter was due to the enhanced fiber reflection.

In a first test, a 1-km length of enhanced scattering fiber was spliced to a 40-km length of standard single-mode fiber (SMF-28). A raw OTDR trace from the DAS system was recorded. The result is shown in Figure 6. Unlike the OTDR traces shown in Figures 1 and 2, the backscattered intensity and phase vary randomly from point to point along the fiber. This is because the DAS interrogator provides high optical coherence within the interrogation pulse and the random phase and amplitude of all of the reflections arising from the disordered molecular structure within an instantaneously illuminated length of the fiber must be added vectorially to produce the resultant intensity at each fiber location. The enhanced scattering fiber gives a signal that is comparable in both magnitude and spatial variability with the unattenuated signal at the input of the 40 km of SMF-28 lead in fiber. This plot demonstrates that the enhanced fiber provides increased optical

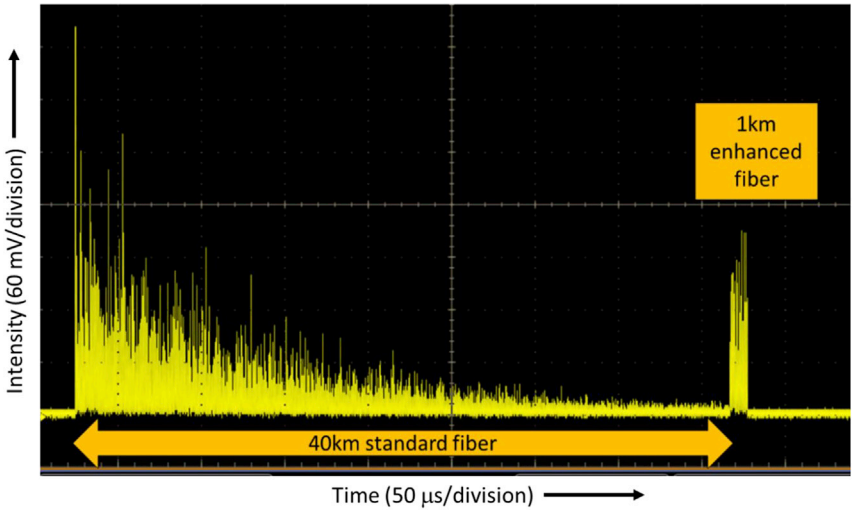

Figure 6. Raw DAS Backscatter Signal of a 1-km Enhanced Scattering Fiber after a 40-km SMF-28 Lead-In Fiber
SMF-28 attenuation is apparent in the decline of signal over the 40 km. The backscatter intensity within the enhanced fiber after the 40-km SMF-28 lead-in fiber is similar to that returned by the SMF-28 at the launch point.

signal to noise within the DAS system while largely preserving the randomness of the spatial intensity and phase variations that are an intrinsic part of phase-sensitive OTDR. In subsequent measurements, this raw signal was converted to measurements of acoustic signals.

The intensity-based interrogation system was characterized using two metrics: system sensitivity and acoustic signal-to-noise ratio. System sensitivity is defined here as the noise equivalent drive amplitude to the piezoelectric tube. Acoustic signal-to-noise ratio (ASNR) is defined as the ratio of the root-mean-square intensity signal amplitude for an optical phase disturbance of approximately 20π radians peak to peak, divided by the intensity noise. This second parameter may be loosely interpreted as the dynamic range of the detection system.

Figure 7 Compares intensity-based amplitude only DAS measurements made using SMF-28 fiber and the enhanced fiber. The plots show raw photodetector signals from the intensity-based system for qualitative comparisons of signals from the enhanced scattering and SMF-28 fibers at examples of short and long range. The DAS signals were generated by driving the exciter at 20 Hz with phase amplitude slightly less than 2π radians peak to peak. The distortion of the intensity signal near to the negative peak excitation shown in the result from the enhanced scattering fiber in Figure 7A is caused by the mean bias phase lying at a slightly negative value rather than precisely at zero. Negative half cycles of phase excitation are driving the intensity signal slightly past the turning point at zero intensity. Table 2 presents the results. For the intensity-based system at 1 km range, the enhanced scattering fiber shows respective benefits of about 12 and 15 dB in sensitivity and acoustic signal-to-noise ratio, respectively, compared with SMF-28 fiber. The phase-based system gained an improvement of about 6 dB in phase noise at 1 km. When used with a 40-km SMF-28 lead-in fiber, the enhanced scattering fiber provides system performance close to that of the SMF-28 fiber at 1 km. For either the phase or intensity-based systems, the improvement in sensitivity realized by use of the enhanced scattering fiber is equivalent to about 33 dB at 41 km range.

Figure 8 shows examples of disturbance waveforms recorded by the phase-based interrogation system at 41 km range. When using SMF-28 fiber, the backscatter is too weak to allow accurate phase recovery, whereas the enhanced scattering fiber provides a much stronger optical signal that supports phase recovery with low noise, accurately reflecting the true waveform of the vibrational disturbance.

Finally, Figure 9 shows measurements from the phase-based interrogation system with a 2-m spatial resolution at a range of 5 km. In this figure, the root-mean-square phase variation is plotted as a function of position along a length of about 67 m spanning a connection between SMF-28 standard single-mode fiber on the left and enhanced scattering fiber on the right. The first 23 m of the enhanced scattering fiber comprises

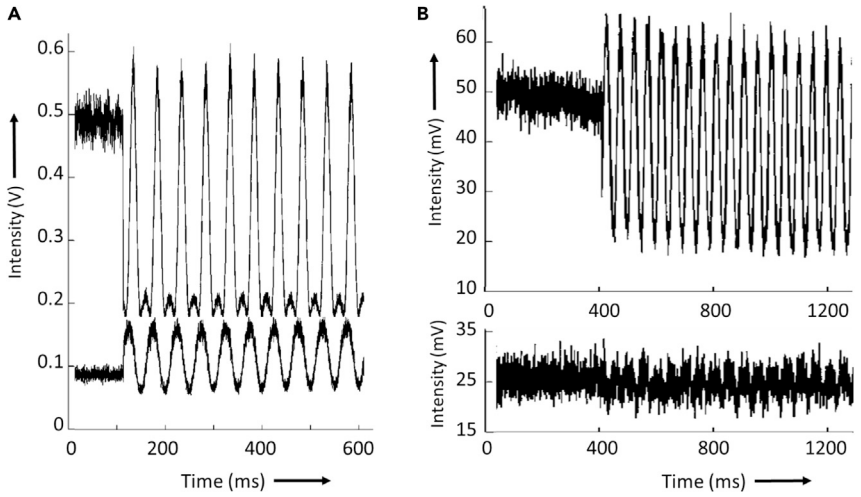

Figure 7. Example Intensity Waveforms with Excitation < 2π Radians

Upper curves from enhanced scattering fiber and lower curves from SMF-28 fiber.

(A) A 1-km range with enhanced scattering fiber throughout. (B) A 41-km range with 40-km SMF-28 lead-in fiber and 1-km enhanced scattering fiber at end.

the PZT exciter used for other tests and the remainder of the enhanced scattering fiber is undisturbed. In this test, the low scattering efficiency of the SMF-28 standard single-mode fiber does not permit reliable phase recovery and so the phase noise is very large and variable from point to point along the fiber. However, once the interrogation pulses enter the enhanced backscatter fiber, phase recovery is achieved with low noise, allowing the ~2.5 radians rms applied disturbance to be easily distinguished from the low, stable background noise level. These results indicate an improvement of 39 dB in signal-to-noise ratio under the test conditions and show the possibility of improved spatial resolution resulting from the use of the enhanced scattering fiber.

Limitations of the Study

The measurements in this work provide significant support for the use of enhanced scattering fibers in sensing applications. Certain limitations to our current work can point to further studies that could underpin their use in additional applications. Although we gave measurements of the instantaneous nonlinear Kerr effect in our work, nonlinear limitations in enhanced scattering fibers associated with Raman and Brillouin scattering were not reported. Thermal reliability measurements over longer timescales and higher temperatures than those that we have reported here can support the use of enhanced fibers under more harsh conditions. The effect of hydrogen on our fibers was not reported in this work. Exposure to sources of hydrogen can be of significance owing to the large attenuation that can be induced by hydrogen exposure in harsh environments such as oil and gas wells. Finally, our distributed acoustic sensor testing showed the possibility of improved spatial resolution. We expect that further experiments will show direct use in high-spatial-resolution applications.

	1-km Range			41-km Range		
	Phase Noise (rad rms)	ASNR	Sensitivity (mV p-p)	Phase Noise (rad rms)	ASNR	Sensitivity (mV p-p)
Enhanced scattering fiber	0.0235	183	5.7	0.047	25.1	17.8
SMF-28 fiber	0.0485	30	24.1	1.81	4.0	835
Improvement (dB)	6.3	15.7	12.5	31.8	16.0	33.4

Table 2. Performance Results for SMF-28 and Enhanced Scattering Fibers

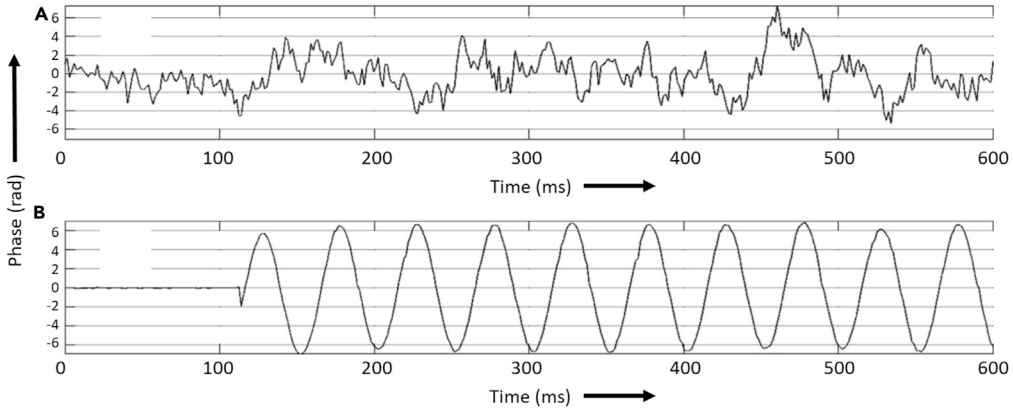

Figure 8. Example Phase Recovered Waveforms at 41 km Range with Excitation ~4π Radians Peak-to-Peak (p-p)
(A) SMF-28 fiber throughout. (B) A 40-km SMF-28 lead-in fiber and 1-km enhanced scattering fiber at end.

Resource Availability

Lead Contact

Further information and requests for resources should be directed to the Lead Contact, Paul Westbrook (westbrook@ofsoptics.com).

Materials availability

No newly generated materials were generated during this study.

Data and code availability

No code was generated in this study and requests for data may be directed to the lead author.

Conclusion

We have described the properties and applications of a new type of sensor fiber that exceeds the limits set by optical fiber Rayleigh scattering. Using a figure of merit comparing backscattering and attenuation we

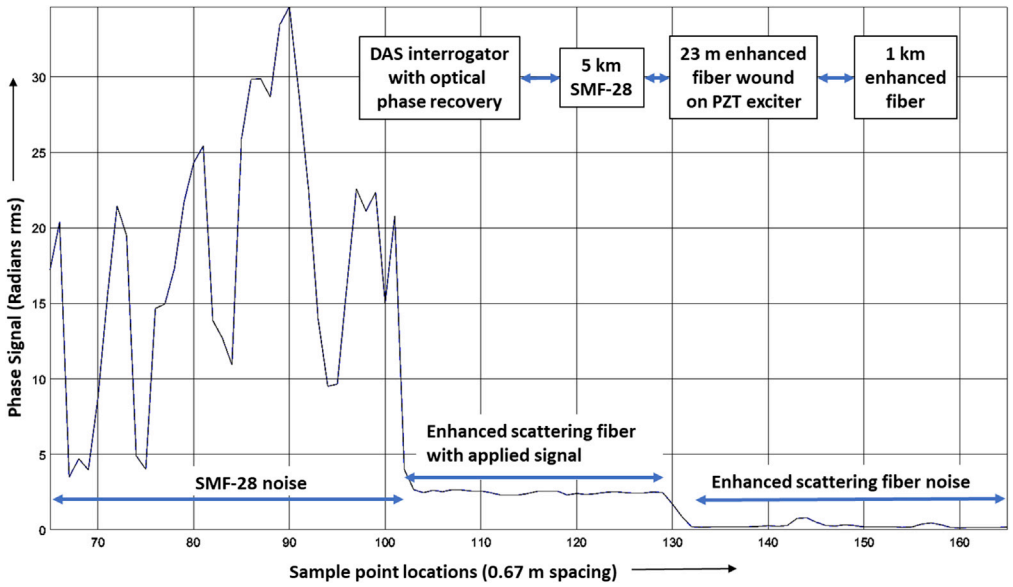

Figure 9. Section of Fiber Path Taken at 5-km Range and 2-m Spatial Resolution
The enhanced scatter fiber shows a benefit of approximately a linear factor of 92x in system sensitivity compared with SMF-28, equivalent to an improvement of ~39 dB.

have shown an improvement of more than one order of magnitude over standard fiber over lengths in excess of 1 km. We have also shown that the enhanced scatter can persist for more than 3 weeks at temperatures in excess of 200°C and anticipate a lifetime in excess of 1 year at temperatures at or below 130°C. A characterization of the nonlinearities of our fiber shows that the Kerr nonlinearity as characterized by the value of n_2 remains within 10% of the value in an unprocessed fiber, both inside and outside the bandwidth of the enhanced scattering. We have also shown that the enhancement can be increased along the length of the optical fiber, thus making the fiber effectively transparent for optical scattering measurements. We were able to show that a 10-fold increase in optical signal to noise can translate to more than 30 dB sensitivity improvement in phase-sensitive DAS measurements of acoustic perturbations. The enhanced scatter fiber promises to have significant impact in the use of DAS throughout many industries.

AUTHOR CONTRIBUTIONS

P.S.W. was the primary author of the manuscript and lead the research effort. V.A.H. lead the DAS research and was responsible for the section on application to DAS measurements. K.S.F., E.M.M., H.W., L.H., D.A.S., and P.S.W. were responsible for the design and fabrication of the enhanced scattering fiber samples. T.K. was responsible for the theoretical analysis. K.S.F., B.Z. and S.S. were responsible for measurements of the enhanced fiber. V.A.H., M.K., A.N., A.Y. were responsible for the DAS measurements.

DECLARATION OF INTERESTS

At the time this work was completed, the following authors were employed by OFS Fitel: P.S.W., K.S.F., T.K., E.M.M., H.W., B.Z., L.H., D.A.S., and S.S. At the time this work was completed the following authors were employed by Fotech Solutions Ltd: V.A.H., M.K., A.N., and A.Y. At present, the following author is employed by Legrand, North America: L.H. The following authors are listed as inventors on US Patent 9,766,396: P.S.W. and T.K. The following author is listed as an inventor on US Patent 9,304,017: V.A.H.

Received: October 23, 2019
Revised: February 25, 2020
Accepted: April 29, 2020
Published: June 26, 2020

REFERENCES

Ahmad, R., Westbrook, P.S., Ko, W., and Feder, K.S. (2019). Probing micron-scale distributed contortions via a twisted multicore optical fiber. APL Photon. *4*, 066101.

Askins, C.G., and Putnam, M.A. (1997). Photodarkening and photobleaching in fiber optic Bragg gratings. J. Lightwave Technol. *15*, 1363–1370.

Askins, C.G., Putnam, M.A., Williams, G.M., and Friebele, E.J. (1994). Stepped-wavelength optical-fiber Bragg grating arrays fabricated in line on a draw tower. Opt. Lett. *19*, 147–149.

Asseh, A., Storoy, H., Sahlgren, B.E., Sandgren, S., and Stubbe, R.A. (1997). A writing technique for long fiber Bragg gratings with complex reflectivity profiles. J. Lightwave Technol. *15*, 1419–1423.

Atkins, R.M., Hale, A., Houlihan, F.M., Kuck, V.J., Olsson, R.T., Paczkowski, M.A., and Simoff, D.A. (2002). Formation of gratings in optical fibers coated with UV-curable polymer. U.S. Patent 6,396,983.

Bai, W., Yu, H., Jiang, D., and Yang, M. (2015). All fiber grating (AFG): a new platform for fiber optic sensing technologies. In 24th International Conference on Optical Fibre Sensors 9634, 96342A.

Bao, X., and Chen, L. (2012). Recent progress in distributed fiber optic sensors. Sensors *12*, 8601–8639.

Bartelt, H., Schuster, K., Unger, S., Chojetzki, C., Rothhardt, M., and Latka, I. (2007). Single-pulse fiber Bragg gratings and specific coatings for use at elevated temperatures. Appl. Opt. *46*, 3417–3424.

Boskovic, A., Chernikov, S.V., Taylor, J.R., Gruner-Nielsen, L., and Levring, O.A. (1996). Direct continuous-wave measurement of n_2 in various types of telecommunication fiber at 1.55 μm. Opt. Lett. *21*, 1966–1968.

Bostick, F.X., III (2000). Field experimental results of three-component fiber-optic seismic sensors. In SEG Technical Program Expanded Abstracts 2000, pp. 21–24.

Brennan, J.F., Matthews, M.R., Dower, W.V., Treadwell, D.J., Wang, W., Porque, J., and Fan, X. (2003). Dispersion correction with a robust fiber grating cover the full c-band at 10-gb/s rates with< 0.3-dB power penalties. IEEE Photon. Technology Lett. *15*, 1722–1724.

Cedilnik, G., Hunt, R., and Lees, G. (2018). Advances in train and rail monitoring with DAS. In Optical Fiber Sensors, ThE35 (Optical Society of America). https://doi.org/10.1364/OFS.2018.ThE35.

Daley, T.M., Freifeld, B.M., Ajo-Franklin, J., Dou, S., Pevzner, R., Shulakova, V., Kashikar, S., Miller, D.E., Goetz, J., Henninges, J., and Lueth, S. (2013). Field testing of fiber-optic distributed acoustic sensing (DAS) for subsurface seismic monitoring. Lead. Edge *32*, 699–706.

Daley, T.M., Miller, D.E., Dodds, K., Cook, P., and Freifeld, B.M. (2016). Field testing of modular borehole monitoring with simultaneous distributed acoustic sensing and geophone vertical seismic profiles at Citronelle, Alabama. Geophys. Prospecting *64*, 1318–1334.

Diamandi, H.H., London, Y., Bashan, G., and Zadok, A. (2019). Distributed opto-mechanical analysis of liquids outside standard fibers coated with polyimide. APL Photon. *4*, 016105.

Duncan, R.G., Froggatt, M.E., Kreger, S.T., Seeley, R.J., Gifford, D.K., Sang, A.K., and Wolfe, M.S. (2007). High-accuracy fiber-optic shape sensing. In Sensor Systems and Networks: Phenomena, Technology, and Applications for NDE and Health Monitoring 2007 6530, p. 65301S, https://doi.org/10.1117/12.720914.

Eickhoff, W., and Ulrich, R. (1981). Optical frequency domain reflectometry in single-mode fiber. Appl. Phys. Lett. *39*, 693–695.

Erdogan, T., Mizrahi, V., Lemaire, P.J., and Monroe, D. (1994). Decay of ultraviolet-induced fiber Bragg gratings. J. Appl. Phys. *76*, 73–80.

Froggatt, M., and Moore, J. (1998). High-spatial-resolution distributed strain measurement in optical fiber with Rayleigh scatter. Appl. Opt. *37*, 1735–1740.

Gander, M.J., MacPherson, W.N., McBride, R., Jones, J.D.C., Zhang, L., Bennion, I., Blanchard, P.M., Burnett, J.G., and Greenaway, A.H. (2000). Bend measurement using Bragg gratings in multicore fibre. Electron. Lett. *36*, 120–121.

Gifford, D.K., Soller, B.J., Wolfe, M.S., and Froggatt, M.E., (2005). Distributed fiber-optic temperature sensing using Rayleigh backscatter. In 2005 31st European Conference on Optical Communication. ECOC Vol. 3, 511-512 IET.

Guo, H., Tang, J., Li, X., Zheng, Y., Yu, H., and Yu, H. (2013). On-line writing identical and weak fiber Bragg grating arrays. Chin. Opt. Lett. *11*, 030602.

Handerek, V. (2016). Distributed optical fibre sensor. U.S. Patent 9,304,017.

Handerek, V.A., Karimi, M., Nkansah, A., Yau, A., Westbrook, P.S., Feder, K.S., Ortiz, R.M., Kremp, T., Monberg, E.M., Wu, H., and Simoff, D.A. (2018). Improved optical power budget in distributed acoustic sensing using enhanced scattering optical fibre. In Optical Fiber Sensors TuC5 (Optical Society of America). https://doi.org/10.1364/OFS.2018.TuC5.

Hartog, A.H. (2017). An Introduction to Distributed Optical Fibre Sensors (CRC press).

Hartog, A., Frignet, B., Mackie, D., and Clark, M. (2014). Vertical seismic optical profiling on wireline logging cable. Geophys. Prospecting *62*, 693–701.

Kanellopoulos, S.E., and Shatalin, S.V. (2012). Detecting a disturbance in the phase of light propagating in an optical waveguide. U.S. Patent 8,264,676.

Kirkendall, C.K., Bartolo, R., Salzano, J., and Daley, K. (2007). Distributed fiber optic sensing for Homeland Security. NRL Rev. 195–196. https://apps.dtic.mil/docs/citations/ADA518230.

Koyamada, Y., Imahama, M., Kubota, K., and Hogari, K. (2009). Fiber-optic distributed strain and temperature sensing with very high measurand resolution over long range using coherent OTDR. J. Lightwave Technol. *27*, 1142–1146.

Lefebvre, P., Vincelette, A., Beaulieu, C., and Ficocelli, P. (2006). Automated manufacturing of fiber Bragg grating arrays. In Optical Fiber Sensors, ThE27 (Optical Society of America). https://doi.org/10.1364/OFS.2006.ThE27.

Lindsey, N.J., Martin, E.R., Dreger, D.S., Freifeld, B., Cole, S., James, S.R., Biondi, B.L., and Ajo-Franklin, J.B. (2017). Fiber-optic network observations of earthquake wavefields. Geophys. Res. Lett. *44*, 11792–11799.

Loranger, S., Gagné, M., Lambin-Iezzi, V., and Kashyap, R. (2015). Rayleigh scatter based order of magnitude increase in distributed temperature and strain sensing by simple UV exposure of optical fibre. Sci. Rep. *5*, 11177.

Lu, P., Mihailov, S.J., Coulas, D., Ding, H., and Bao, X. (2019). Low-loss random fiber gratings made with an fs-IR laser for distributed fiber sensing. J. Lightwave Technol. *37*, 4697–4702.

Mateeva, A., Lopez, J., Potters, H., Mestayer, J., Cox, B., Kiyashchenko, D., Wills, P., Grandi, S., Hornman, K., Kuvshinov, B., and Berlang, W. (2014). Distributed acoustic sensing for reservoir monitoring with vertical seismic profiling. Geophys. Prospecting *62*, 679–692.

Monet, F., Loranger, S., Lambin-Iezzi, V., Drouin, A., Kadoury, S., and Kashyap, R. (2019). The ROGUE: a novel, noise-generated random grating. Opt. Express *27*, 13895–13909.

Nakazawa, M. (1983). Rayleigh backscattering theory for single-mode optical fibers. J. Opt. Soc. Am. *73*, 1175–1180.

Owen, A., Duckworth, G., and Worsley, J. (2012). OptaSense: Fibre optic distributed acoustic sensing for border monitoring. In 2012 European Intelligence and Security Informatics Conference, 362-364.

Parker, T., Shatalin, S., and Farhadiroushan, M. (2014). Distributed Acoustic Sensing–a new tool for seismic applications. First Break *32*, 61–69.

Personick, S.D. (1977). Photon probe—an optical-fiber time-domain reflectometer. Bell Syst. Tech. J. *56*, 355–366.

Posey, R., Johnson, G.A., and Vohra, S.T. (2000). Strain sensing based on coherent Rayleigh scattering in an optical fibre. Electro. Lett. *36*, 1688–1689.

Sancho, J., Chin, S., Barrera, D., Sales, S., and Thévenaz, L. (2013). Time-frequency analysis of long fiber Bragg gratings with low reflectivity. Opt. Express *21*, 7171–7179.

Shatalin, S.V., Treschikov, V.N., and Rogers, A.J. (1998). Interferometric optical time-domain reflectometry for distributed optical-fiber sensing. Appl. Opt. *37*, 5600–5604.

Soller, B.J., Gifford, D.K., Wolfe, M.S., and Froggatt, M.E. (2005). High resolution optical frequency domain reflectometry for characterization of components and assemblies. Opt. Express *13*, 666–674.

Tanimola, F., and Hill, D. (2009). Distributed fibre optic sensors for pipeline protection. J. Nat. Gas Sci. Eng. *1*, 134–143.

Wang, Z.N., Zeng, J.J., Li, J., Fan, M.Q., Wu, H., Peng, F., Zhang, L., Zhou, Y., and Rao, Y.J. (2014). Ultra-long phase-sensitive OTDR with hybrid distributed amplification. Opt. Lett. *39*, 5866–5869.

Wellbrock, G.A., Xia, T.J., Huang, M.F., Chen, Y., Salemi, M., Huang, Y.K., Ji, P., Ip, E., and Wang, T. (2019). First field trial of sensing vehicle speed, density, and road conditions by using fiber carrying high speed data. In 2019 Optical Fiber Communications Conference and Exhibition, pp. 1–3.

Westbrook, P.S.. (2016). Optical sensor having fiduciary marks detected by Rayleigh scattered light. U.S. Patent 9,470,588.

Westbrook, P. (2020). Big data on the horizon from a new generation of distributed optical fiber sensors. APL Photon. *5*, 020401.

Westbrook, P.S., Feder, K.S., Kremp, T., Taunay, T.F., Monberg, E., Kelliher, J., Ortiz, R., Bradley, K., Abedin, K.S., Au, D., and Puc, G. (2014). Integrated optical fiber shape sensor modules based on twisted multicore fiber grating arrays. In Optical Fibers and Sensors for Medical Diagnostics and Treatment Applications XIV, *8938*Optical Fibers and Sensors for Medical Diagnostics and Treatment Applications XIV, p. 89380H, https://doi.org/10.1117/12.2041775.

Westbrook, P.S., Feder, K.S., Kremp, T., Taunay, T.F., Monberg, E., Puc, G., and Ortiz, R. (2015). Multicore optical fiber grating array fabrication for medical sensing applications. In Optical Fibers and Sensors for Medical Diagnostics and Treatment Applications XV, *9317*Optical Fibers and Sensors for Medical Diagnostics and Treatment Applications XV, p. 93170C, https://doi.org/10.1117/12.2077833.

Westbrook, P.S., Kremp, T., Feder, K.S., Ko, W., Monberg, E.M., Wu, H., Simoff, D.A., Taunay, T.F., and Ortiz, R.M. (2017a). Continuous multicore optical fiber grating arrays for distributed sensing applications. J. Lightwave Technol. *35*, 1248–1252.

Westbrook, P.S., Feder, K.S., Ortiz, R.M., Kremp, T., Monberg, E.M., Wu, H., Simoff, D.A., and Shenk, S. (2017b). Kilometer length, low loss enhanced back scattering fiber for distributed sensing. In 2017 25th Optical Fiber Sensors Conference Post Deadline Papers, 1-5.

Zaitsev, I.A., Butov, O.V., Voloshin, V.V., Vorob'ev, I.L., Vyatkin, M.Y., Kolosovskii, A.O., Popov, S.M., and Chamorovskii, Y.K. (2016). Optical fiber with distributed Bragg-type reflector. J. Commun. Technol. Electron. *61*, 639–645.